Coherent x-ray diffraction imaging of ZnO nanostructures under confined illumination

2011 New J. Phys. 13 033006

(http://iopscience.iop.org/1367-2630/13/3/033006)

New Journal of Physics
The open-access journal for physics

Coherent x-ray diffraction imaging of ZnO nanostructures under confined illumination

Gang Xiong[1,5], Xiaojing Huang[1,2], Steven Leake[1,3], Marcus C Newton[1], Ross Harder[2] and Ian K Robinson[1,4]

[1] London Centre for Nanotechnology, University College London, London WC1H 0AH, UK
[2] Advanced Photon Source, Argonne, IL 60439, USA
[3] Swiss Light Source, Villigen, Switzerland
[4] UK and Diamond Light Source, Harwell Campus, Didcot, Oxfordshire OX11 0DE, UK
E-mail: ganxiong@hotmail.com

New Journal of Physics **13** (2011) 033006 (11pp)
Received 16 November 2010
Published 2 March 2011
Online at http://www.njp.org/
doi:10.1088/1367-2630/13/3/033006

Abstract. Coherent x-ray diffraction imaging has been used to study a single ZnO nanorod in a confined illuminating condition. The focused beam size is smaller than the length of the nanorod, and the diffraction intensity is strongly dependent on the illumination position. The density maps show that the nanorod width in the radial direction is around 210 nm and has a length of 1.5 μm, in agreement with the scanning electron microscope measurement. Reconstructed phase maps show a maximum phase change of 0.8 radians. The reconstructed direct space structures reveal the exit wavefront profile, which includes that of the focused x-ray beam. The beam profile presents in reconstructions some 'hill and valley' surface features with a typical size of a few tens of nanometres and are attributed to the noise due to the slow variation of the focused beam intensity along the boundary. A single ZnO tetrapod has been investigated with the same method to recover the beam profile in the horizontal direction.

[5] Author to whom any correspondence should be addressed.

Contents

1. Introduction

X-ray diffraction methods are favourable for the *in situ* measurement of strain distributions on the nanoscale because of their non-destructive nature and sensitivity to sub-Ångstrom lattice distortion. Several variants have been demonstrated to date. For example, the isostrain method [1] has been extensively used for studying pattern formation in epitaxial systems of semiconductors, a prominent example being Ge on Si with a 4% lattice mismatch, to investigate the critical-thickness effect in which a maximum thickness of strained material can form when there is a lattice mismatch between a thin film of one semiconductor and its substrate [2]. Another method, the high-resolution x-ray diffraction [3], has been carried out on beamline BM32 at the European Synchrotron Radiation Facility (ESRF) in Grenoble, indirectly examining the strain distributions in lithographically prepared micrometre-sized structures, consisting of patterned Si wire structures engraved in silicon-on-insulator layers as arrays to enhance the signal. Finite-element analysis methods were used to model the strain, a kinematical diffraction calculation of the strained wires followed, and the results were found to be in good agreement with the experimental data [4].

It is necessary for the above methods to illuminate a vast number of equivalent samples simultaneously, i.e. the diffracted intensity is sample averaged in order to measure the diffracted intensity with sufficient statistical accuracy. When fabricated, the elements have to be made with the same shape and similar size, with identical orientation on the substrate. This limitation can be overcome by the recent development of coherent x-ray diffraction imaging (CXDI) which examines a single, isolated sample [5]–[8].

2. Coherent x-ray diffraction imaging

CXDI is normally carried out with the whole crystal illuminated by a spatially coherent beam of x-rays, so the transverse coherence length (up to a few micrometres) exceeds the dimensions of the crystal [7]. Scattering from the entire volume of the crystal at the Bragg reflection condition will interfere in the far-field, producing a three-dimensional (3D) diffraction pattern in reciprocal space. The scattered amplitude is a complex quantity, $A = |A| \exp(\mathrm{i}\varphi)$, and by inverting the amplitude back to direct space using phase retrieval algorithms, one can obtain the complex 3D electron density of the illuminated crystal. The Q-vector is known and remains approximately constant for the measurement, thus in direct space the phase (ϕ) of the complex density describes the displacement of the crystal planes parallel to the Q-vector, $\phi = \boldsymbol{Q}.\boldsymbol{r}$.

In experiments, the diffracted intensity is measured using a charge coupled device (CCD) area detector, positioned far enough away to resolve the finest fringes of the diffraction pattern.

However, as only the intensities ($I = |A|^2$) of the continuous diffraction pattern are measured, the phase information is lost, which gives rise to a 'phase problem'. To recover the phases from the measured intensity, the diffraction pattern must be sampled at greater than the Nyquist frequency for the size of the crystal. This oversampling condition is simply that the number of measurement points be at least twice the number of unknown density points. Phasing is achieved by a combination of the hybrid input output (HIO) algorithm, the error reduction (ER) algorithm, and a 'support' constraint, in which all the complex electron density is constrained to exist and whose dimensions can be estimated directly from the fringe spacing of the observed pattern or using autocorrelation methods. The principal operation encompasses an iterative loop between the experimentally measured intensity distribution and the direct space crystal to be imaged, traversed via discrete Fourier transformation. These steps are usually sufficient to find a unique set of phases consistent with the measured amplitude and support constraints after a number of iterative loops of direct and inverse Fourier transformation, i.e. CXDI has the potential to refine the electron density distribution in a more or less model-independent way [8, 9].

CXDI is becoming a powerful technique for the structural characterization of nanosized devices [10]. The main advantage for the investigation of nanostructures is that it provides 3D quantitative phase information which is sensitive to lattice distortions (related to strain) [11]–[14]. This method has been employed to recover 3D images from a single Bragg reflection of a lead nanocrystal [11] and a gold nanocrystal [15] and more recently to map 3D strain field distributions from multiple Bragg reflections of a single ZnO crystal [16].

In traditional CXDI measurements, the beam spot (also called the 'probe') size exceeds the dimensions of the sample. We report here the study of applying CXDI on a single ZnO nanorod/tetrapod under confined illumination conditions, with one dimension of the sample larger than the beam spot. The resulting images illustrate that, when measured from the ZnO nanorod/tetrapod base rod, the focused beam is cutting through the rod/tetrapod, while when moved away from the centre, it starts illuminating one of the ends of the crystal. We present the first attempt to image the beam wavefront profile in one dimension with this confined illumination setup. Probe retrieval by inversion of diffraction patterns has traditionally been hard to achieve because of the inherent soft edges and the lack of information from measured data. As we will demonstrate, the edges of the beam can be visualized in one direction by the same methods that work well for compact objects. This represents a step towards CXDI determination of the wavefront profile of the focused beam, which is of importance to a number of potential applications where precise knowledge of the probe is critical for scanning methods on samples bigger than the beam, such as ptychography, which solves the diffraction-pattern phase problem by interfering adjacent Bragg reflections coherently and thus determining their relative phase.

3. Methods and experiments

ZnO is an important electronic and photonic material due to its wide direct band gap of 3.37 eV. It has a fairly large excitation binding energy (60 meV) and exhibits near-ultraviolet (UV) emission and transparent conductivity at room temperature and above. Since the first report of UV lasing from ZnO nanorods, considerable effort has been devoted to the fabrication and characterization of well defined one-dimensional (1D) ZnO nanostructures with various morphologies, such as nanowires, nanobelts and tetrapods. Functional devices such as piezoelectric nanogenerators, optically pumped nanolasers, solar cells and field emission

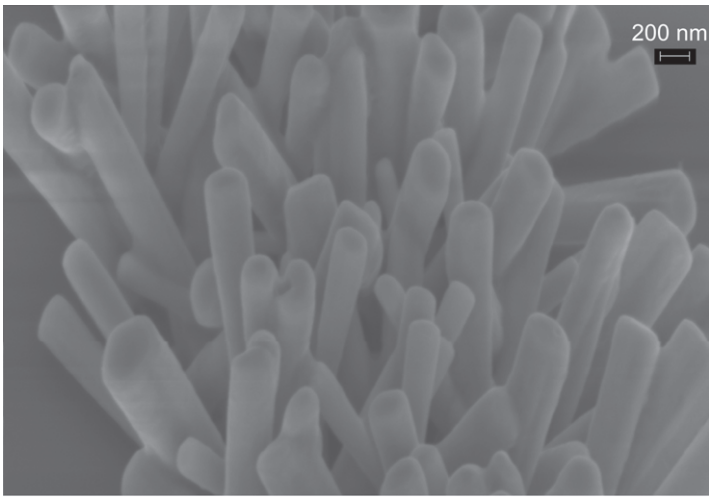

Figure 1. SEM image of the ZnO nanorods grown using the CVTD method (substrate tilted 45° for the imaging).

devices have already been demonstrated [17]–[19]. Here, ZnO rods and tetrapod-shaped nanocrystals were synthesized via a chemical vapour deposition technique. A Si wafer with (111) orientation was diced into $8 \times 8\,\mathrm{mm}^2$ dice and cleaned in acetone and isopropyl-alcohol in an ultrasonic bath for 5 min separately, then blown dry with N_2. Electron beam lithography was then used to pattern micro-sized strips of aluminium to a depth of 6–10 nm on the cleaned Si substrate by sputter deposition. This was used to form catalyst centres that seed the growth of ZnO nanorods. High-purity zinc powder (99.9999%) was used as a source material and was placed in an alumina boat in the centre of a quartz tube. Aluminium patterned Si substrates were then placed 2 cm downstream of the alumina boat, and the quartz tube inserted into a thermal tube furnace. The tube was subsequently evacuated to a pressure of 0.5 mbar while a flow rate of 5 sccm oxygen was maintained throughout the experiment. The furnace was heated to 600 °C, at which point Zn vapour was released and oxidized leading to the selective growth of ZnO nanorods. The process was maintained for 3 h after which the furnace was allowed to cool naturally, which produced ZnO nanorods on top of the aluminium stripes, vertical to the substrate, with typical lengths of 1–2 μm and widths of 100–300 nm, as measured by a scanning electron microscope; see figure 1. By adjusting the gas flow rate and the position of the substrate, ZnO tetrapods of similar dimensions were grown on a Si substrate without using an Al catalyst.

Measurements on ZnO nanostructures produced in this way were performed at the Advanced Photon Source (APS) beamline 34-ID-C, Argonne National Laboratory. The beamline consists of an undulator setting the beam energy to 7.2 keV, corresponding to a wavelength of 1.72 Å, a beam-splitting mirror which directs the beam onto a silicon (111) double crystal monochromator, and a set of roller blade slits ($50 \times 50\,\mu\mathrm{m}^2$) defining the coherent beam dimensions in the horizontal and vertical directions. An instrumental combination of horizontal and vertical Kirkpatrick–Baez mirrors further focus the beam to a spot with dimensions around 1 μm. The sample was mounted on translation stages and then moved into the beam, whereby an *in situ* optical confocal microscope pinpointed the exact location of the nanocrystal under study [20]. A stationary CCD detector with pixel size of $22.5 \times 22.5\,\mu\mathrm{m}^2$ was used to sample the diffraction pattern surrounding the chosen Bragg peak at a distance of 0.5 m from the sample.

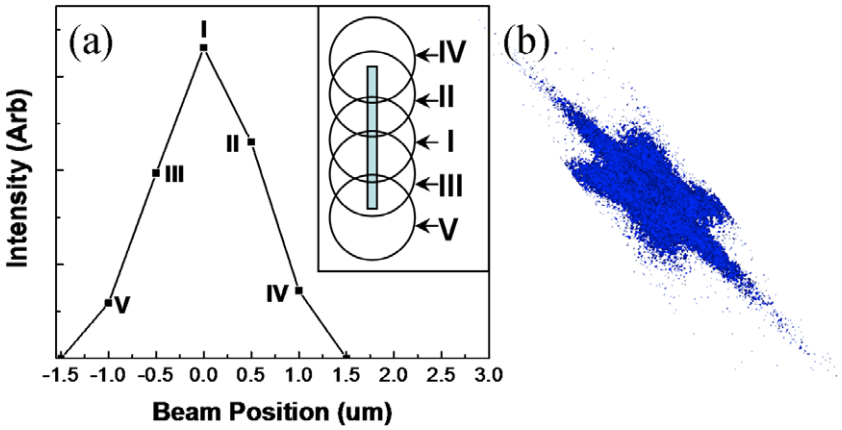

Figure 2. (a) Diffraction intensity dependence on the beam relative positions to the ZnO nanorod (origin is defined as the position where maximum intensity is detected). Inset: schematic view of the relative positions of the x-ray beam to the ZnO nanorod in the series measurements. (b) 3D isosurface diffraction pattern (raw data in pixel coordinates) from beam illumination position I, drawn at 400 ADU.

When the (010) reflection from a ZnO nanorod was located, the sample position was adjusted by moving the stage in steps along X, Y, Z and θ directions, in order to maximize the diffracted intensity. The incident angle of the beam to the substrate was 16°, so the beam direction was nearly perpendicular to the axis of the ZnO nanorod as the rods were perpendicular to the substrate. The position with maximum diffraction intensity corresponded to the focused beam hitting the centre of the nanorod. A series of measurements was performed by adjusting the height of the stage thus moving the nanorod c-axis vertically relative to the beam, with a step size of 0.5 μm. Figure 2(a) shows the diffraction intensity dependence on the illumination position, in which the origin is defined as the illumination position where the maximum intensity was collected, which corresponds to the beam illuminating the rod centre. The inset shows a schematic view of the illumination positions for the measurements. It can be seen that the intensity is strongly dependent on the position, decreasing quickly as the focused beam moved away from the centre position. In addition, when the beam moved more than two steps, i.e. $\geqslant 1.5\,\mu$m from the centre position, the intensity dropped to zero and there was no diffraction pattern visible on the CCD detector. This is understandable given the fact that the nanorod has a length in the range of 1–2 μm and the beam size is around 1 μm. With the beam moving away from the centre position, part of the beam will no longer illuminate the sample, i.e. the sample volume illuminated by the beam has become smaller, thus the diffraction intensity decreases. A distance larger than 1.5 μm away from the nanorod centre would move the beam completely out of the nanorod; thus the diffraction intensity drops to zero.

At each of the five illumination positions shown in the inset of figure 2(a), a complete set of diffraction patterns from the ZnO (010) reflection was collected by rotating the sample through the Bragg conditions in increments of 0.02°. At each step, a two-dimensional (2D) slice of the diffraction pattern was acquired by the direct-detection CCD and was subsequently collated, to form a complete 3D diffraction pattern. Figure 2(b) is a complete 3D ZnO (010) Bragg diffraction pattern collected at illumination position I by collating a full set of 2D slices

of the diffraction pattern, which consisted of 70 slices with a total rotation angle of 1.4°. The isosurface of the diffraction pattern, with constant amplitude, is drawn at 400 analogue digital units (ADU), just above the background noise in order to remove the read-out error in the CCD. It reveals the six-fold symmetric plane of von Laue fringes, representing the hexagonal crystal shape of the ZnO nanorod.

Using a combination of the HIO and the ER algorithm, with a support constraint in direct space, the diffraction patterns can be successfully transformed back to reveal the crystal density distribution in direct space after 150 iterations [21]. Figures 3(a)–(c) show the isosurface of the reconstructed density maps of the nanorod using diffraction data of the (010) Bragg reflection collected at positions I, II and III (as schematically shown in the inset of figure 2(a)). The inset in figure 3 is a scalar cut plane image along the radial direction of the reconstructed density map. It can be seen that the density images appear as a hexagonal rod-shaped crystal with slightly round edges, with diameters in the range of 205–215 nm at positions along the rod, and the distance between the two ends from 780 to 1100 nm, depending on the measurement position. With illumination position I, in which the focused beam is located in the middle of the rod, the density map shows the longest distance to be 1.1 μm; this is actually the size of the focused beam along the rod axial direction (figure 3(a)). It can also be seen that both ends are rough. When the beam is 0.5 μm away from the rod centre, the distance between two ends of the reconstructed rod becomes shorter, 830 nm at position II (figure 3(b)) and 780 nm at position III (figure 3(c)), and one end of the rod is rough, while the other end is squarer and smooth in appearance on the isosurface. The results are consistent with the fact that, when measured from the rod centre, the focused beam edges define the crystal size since the beam is smaller than the rod it is cutting through, rather than illuminating the whole crystal. In contrast, when the beam is moved away from the centre, it starts illuminating one of the rod ends and therefore the illuminated part will become shorter. On the reconstructed density contour the rough end is where the beam cut the rod and the smooth end represents the rod end which is illuminated by the coherent beam. Reconstructed density maps from illumination positions at IV and V (not shown here) are similar to those from positions II and III, respectively, and with shorter lengths between the two ends, because the beam spot has been moved further away from the rod centre. As the beam movement step is 0.5 μm and the beam dimension in this direction is 1.1 μm (figure 3(a)), it can be estimated that the nanorod length is around 1.5 μm by superimposing the images of figures 3(a)–(c). Those results are in good agreement with the SEM measurement (figure 1).

Figure 3(a) shows that when the beam is cutting through the nanorod the reconstructed density map has two rough ends, which represent the beam wavefront profile in this confined illumination scanning setup. Figures 4(a) and (b) are zoomed images of the ends of the reconstructed density map from illumination position I, to show the wavefront profile of the focused beam. The recovered beam boundary presents some 'hill and valley' surface roughness structures with typical sizes of a few tens of nanometres. These apparent surface features on the beam wavefront may be attributed to an amplification of noise or errors in the data coupled with the slow variation of the focused beam intensity along the boundary [15]. The surface roughness may come from statistical noise in the data, minor aberrations in the optics, such as slightly asymmetric roller-blade slits or asymmetric KB mirror bending, or phase errors in the beryllium exit window. Those noise sources consequently cause noise in phasing and result in small non-uniqueness in the solution, as evidenced by the fact that, when starting from different random models; solutions present different surface roughness features on the scale

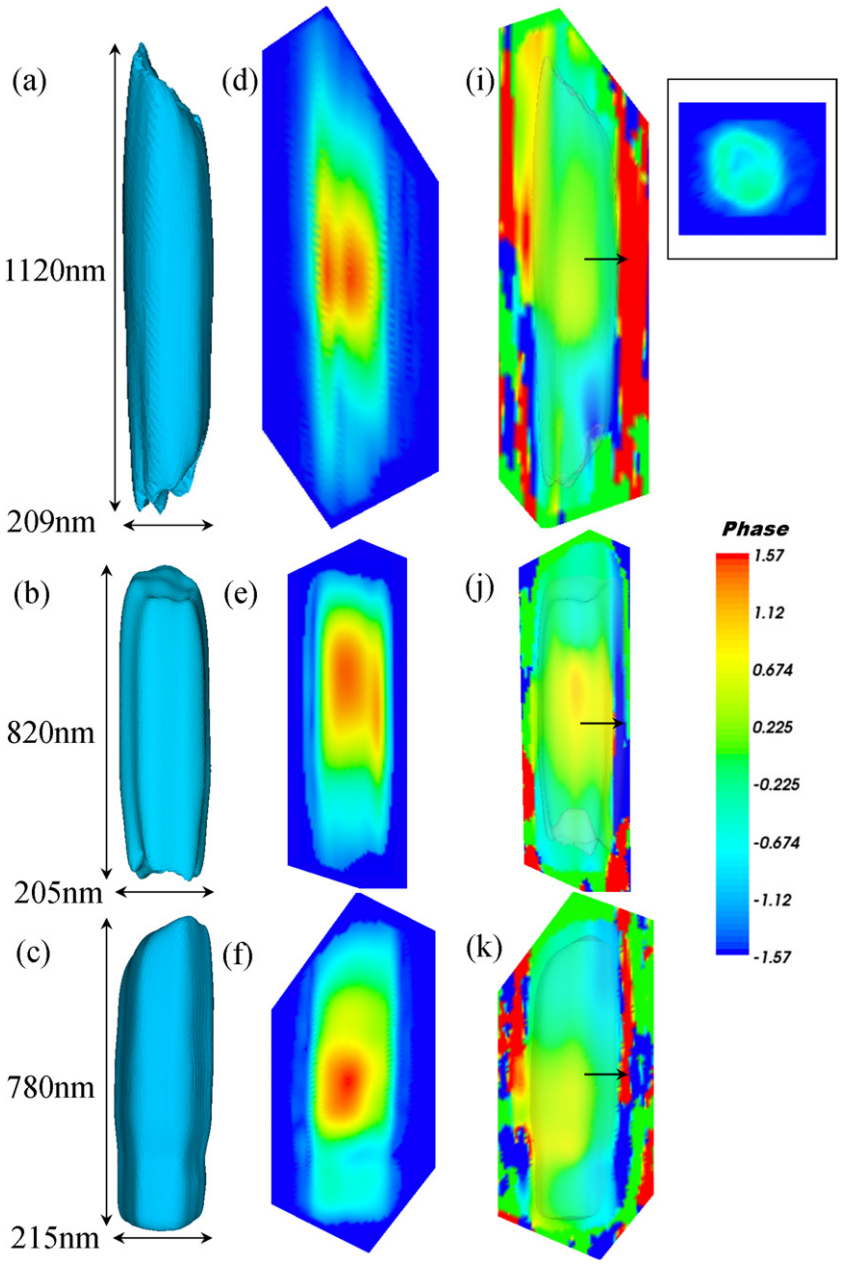

Figure 3. The reconstructed density maps: from illumination positions I—(a), II—(b) and III—(c); the scalar cut plane images along the axial direction of the reconstructed ZnO nanorod density maps: from illumination positions I—(d), II—(e), and III—(f); and the scalar cut plane images along the axial direction of the reconstructed nanorod phase maps, from beam positions I—(i), II—(j) and III—(k). The black arrows indicate the direction of the (010) Q-vector; the inset shows a scalar cut plane image along the radial direction of the reconstructed ZnO nanorod density map, which presents a hexagonal shape with slightly round edges.

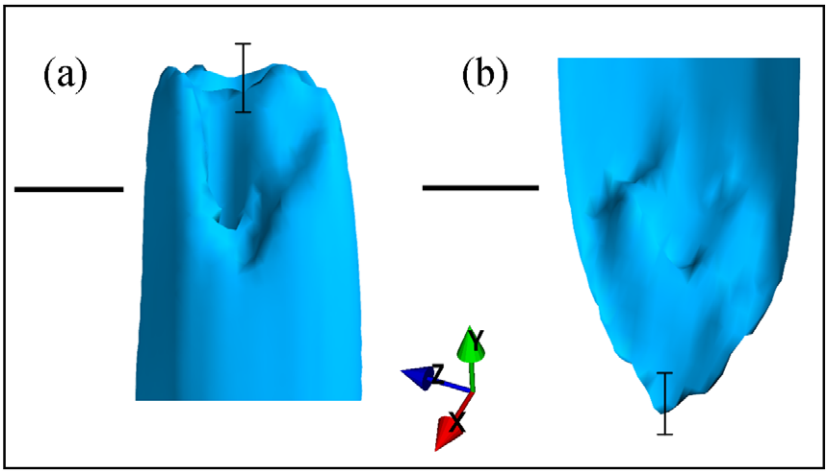

Figure 4. (a, b) Zoomed images of the two ends of the reconstructed ZnO nanorod density map from illumination position I. Scale bar = 100 nm; error bar indicates variation of the boundary position due to different random starting models in the phasing calculations.

of a few tens of nanometres. The error bar in figure 4 indicates the variation of the boundary position due to different random starting models in the phasing calculation. It is known that coherent beams have different focal properties from incoherent ones, as the propagation is better described by its wavefront which consists of surfaces of constant phase. Knowledge of the probe is critical for applications in the high-resolution imaging of a wide variety of samples such as organic tissues and other organic and inorganic specimens. However, in CXDI the reconstructed image is of an exit wave field, which is the product of the illumination wave field and the sample transmission function, both of them complex. Recent progress seen in a ptychography experiment, by varying the sample position systematically with respect to the probe, allowed both the probe and the sample structures to be reconstructed independently [22, 23]. However, this has not been achieved to date in the Bragg geometry. The results here show another way to retrieve the probe wavefront profile by using the confined illumination CXDI.

Figures 3(d)–(f) are the scalar cut plane images along the axis of the reconstructed ZnO nanorod from illumination positions I, II and III, respectively, and are consistent with the corresponding density maps, with two rough ends from illumination position I, one rough end and one smooth end for illumination positions II and III. It can be seen that there is a curved high-density region in the centre of the scalar cut plane images. Features of this type have been observed in reconstructions from other samples [8, 24, 25] and are called 'hot spots'. There are two possible origins for our 'hot spot'. The first one is that the focused beam probe is not perfectly coherent, consisting of a dominant central coherent mode and a number of weaker ones. The diffraction pattern therefore includes a fully coherent component and a background which reduces the visibility. After reconstruction in direct space the solution appears as a low-density full-size representation of the object and a superimposed 'hot spot' [24]. The other possible origin is that it is simply a feature of the ZnO nanorod itself. Completely ruling out one or the other explanation is out of the scope of this paper, and work is in progress in this active area of study.

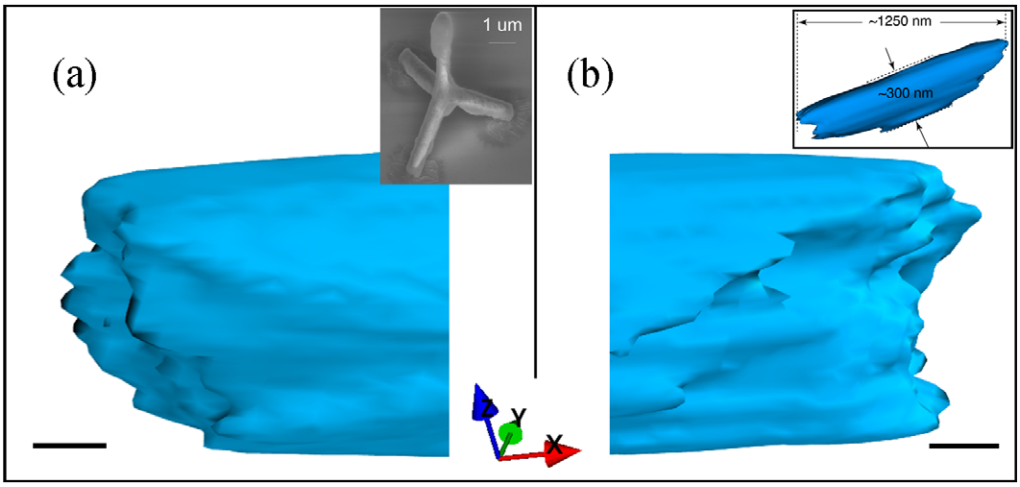

Figure 5. (a, b) Zoomed images of the two ends of the reconstructed density map of a base rod of the ZnO tetrapod. Inset in (a): SEM image of the ZnO tetrapod, inset in (b): reconstructed density map of the ZnO tetrapod base rod. (scale bar = 100 nm)

In the reconstructions here, a real space phase range of ± 1.57 radians was used as a real-space constraint in the phasing algorithms and was found to be sufficient to encompass the data without the occurrence of phase wrapping. Figures 3(i)–(k) are the scalar cut plane images through the axial direction of the reconstructed nanorod phase maps, from the illumination positions of I, II and III, respectively. A semi-transparent isosurface of the 3D density map is superimposed on each phase map to show the reconstructed shape of the nanorod. The colours indicate the variation of the phase inside the nanorod. The colour bar ranges from -1.57 to 1.57 radians on a scale where 2π would represent a displacement of one lattice spacing if the phase were attributed to strain [13]. Note that the phase becomes very noisy outside the nanorod, where the amplitude of the complex density function vanishes and the phase has little meaning. The black arrows indicate the direction of the (010) Q vector used for measuring the diffraction onto which the lattice distortion (strain) is projected. The maximum phase change is around 0.8 radians from figures 3(i)–(k), which would correspond to a maximum displacement of 0.05 nm relative to the ideal crystal lattice, about a seventh of the ZnO (010) lattice spacing. However, it is also possible that the phase is in the probe. Given the similarity of the phase images in figures 3(i)–(k), we think this is more likely to be the case.

Reconstructing the Bragg diffraction pattern from a ZnO nanorod vertically grown on the substrate, with confined illumination, allows us to retrieve the focused beam profiles in the vertical direction. We performed the same measurements on a ZnO tetrapod, which consists of four rod-shaped structures joined at tetrahedral angles to a central core. The ZnO tetrapod is standing with three rods touching a Si substrate, and the other rod vertically pointing upward, as shown in the inset of figure 5(a). The reconstructed density map from one of the base rods in confined illumination is used to recover the beam profiles in the horizontal direction. Figures 5(a) and (b) show the recovered beam profiles, using the reconstructed density map of a base rod of the tetrapod (inset of figure 5(b)). It can be seen that the profiles again show rough curved features, with similar dimensions to the vertical profiles recovered from the ZnO nanorod. The reconstructed density section has a length of 1.25 μm, which is the beam size in

this illumination direction, and is similar to the dimension measured in the vertical direction and that determined for the mirror focus. It is worth noting that in this measurement setup, the base rod is not perfectly horizontal and has a 19° angle to the horizontal direction, so that the reconstructed wavefront profile includes a small vertical component.

4. Conclusions

We have performed CXDI measurements to investigate single ZnO nanorods and tetrapods in a confined illumination condition, using the beamline 34-ID-C at the Advanced Photon Source, Argonne National Laboratory. The coherent x-ray beam was focused to around 1 μm in both directions using a set of roller-blade slits and Kirkpatrick–Baez mirror optics, smaller than the sample size. The diffraction intensity was strongly dependent on the illumination position, with the maximum intensity collected when the beam sat in the middle of the sample, and rapidly dropped off with the beam moving away from the centre and reaching one of the ends. The density maps of the nanorod showed its dimension in the radial direction is around 210 nm and has a length of 1.5 μm, in good agreement with the SEM measurement. It can be seen that there are 'hot spot' features in the density maps, which may be attributed to the partial coherence of the focused beam. The reconstructed phase maps showed a fairly uniform structure, without significant phase ripples or wrapping inside the rod, and a maximum phase change of 0.8 radians. It would correspond to a displacement of 0.05 nm if this were due to strain, which is about a seventh of the lattice parameter along the measured (010) orientation. However, its consistent appearance at multiple positions suggests this is a property of the beam. The reconstructed density map is used to recover the profile of the focused x-ray beam in the vertical direction, which shows some 'hill and valley' surface roughness structures in the surface contour, with typical sizes in the range of a few tens of nanometres. These surface features are attributed to the noises due to the slow variation of the focused beam intensity along the boundary, which consequently causes noises in phasing and results in small non-uniqueness in the solution at the level of the phasing error estimate. A ZnO tetrapod was investigated with this method to recover the beam profile in the horizontal direction, which presents similar roughness features as the one retrieved in the vertical direction from the ZnO nanorod.

Acknowledgments

This project is supported by the European Research Council as an FP7 Advanced grant 'Nanosculpture', code 227711. The measurements were carried out at APS beamline 34-ID-C, built with US National Science Foundation grant DMR-9724294 and operated by the US Department of Energy, Office of Basic Energy Sciences, under contract no. DE-AC02–06CH11357.

References

[1] Metzger T H, Schulli T U and Schmidbauer M 2005 *C. R. Phys.* **6** 47

[2] Malachias A, Kycia S, Medeiros-Ribeiro G, Magalhães-Paniago R, Kamins T I and Williams R S 2003 *Phys. Rev. Lett.* **91** 176101

[3] Gailhanou M, Loubens A, Micha J-S, Charlet B, Minkevich A A, Fortunier R and Thomas O 2007 *Appl. Phys. Lett.* **90** 111914

[4] Minkevich A A, Gailhanou M, Micha J-S, Charlet B, Chamard V and Thomas O 2007 *Phys. Rev.* B **76** 104106
[5] Fienup J R 1982 *Appl. Opt.* **21** 2758
[6] Bates R H T 1982 *Optik* **61** 247
[7] Vander Veen and Pfeiffer F 2004 *J. Phys.: Condens. Matter* **16** 5003
[8] Robinson I K, Vartanyants I A, Williams G J, Pfeifer M A and Pitney J A 2001 *Phys. Rev. Lett.* **87** 195505
[9] Miao J W, Charalambous P, Kirz J and Sayre D 1999 *Nature* **400** 342
[10] Robinson I and Harder R 2009 *Nat. Mater.* **8** 292
[11] Pfeifer M A, Williams G J, Vartanyants I A, Harder R and Robinson I K 2006 *Nature* **42** 63
[12] Miao J W, Hodgson K O, Ishikawa T, Larabell C A, LeGros M A and Nishino Y 2003 *Proc. Natl Acad. Sci. USA* **100** 110
[13] Harder R, Pfeifer M A, Williams G J, Vartaniants I A and Robinson I K 2007 *Phys. Rev.* B **76** 115425
[14] Schroer C G, Boye P, Feldkamp J M, Patommel J, Schropp A, Schwab A, Stephan S, Burghammer M, Schoder S and Riekel C 2008 *Phys. Rev. Lett.* **101** 090801
[15] Williams G J, Pfeifer M A, Vartanyants I A and Robinson I K 2006 *Phys. Rev.* B **73** 094112
[16] Newton M C, Leake S J, Harder R and Robinson I K 2010 *Nat. Mater* **9** 120
[17] Wang Z L and Song J 2006 *Science* **312** 242
[18] Song J, Zhou J and Wang Z L 2006 *Nano Lett.* **6** 1656
[19] Law M, Greene L E, Johnson J C, Saykally R and Yang P 2005 *Nat. Mater.* **4** 455
[20] Beitra L, Watari M, Matsuura T, Shimamoto N, Harder R and Robinson I 2010 *AIP Conf. Proc.* **CP1234** 57
[21] Harder R, Liang M, Sun Y, Xia Y and Robinson I K 2010 *New J. Phys.* **12** 035019
[22] Abbey B, Nugent K A, Williams G J, Clark J N, Peele A G, Pfeifer M A, Jonge M D and Mcnulty I 2008 *Nat. Phys.* **4** 394
[23] Thibault P, Dierolf M, Menzel A, Bunk O, David C and Pfeiffer F 2008 *Science* **321** 379
[24] Vartanyants I A and Robinson I K 2001 *J. Phys.: Condens. Matter* **13** 10593
[25] Leake S J, Newton M C, Harder R and Robinson I K 2009 *Opt. Express* **17** 15853